Multiscale γ variant selection in a quaternary near-γ Ti-Al alloy

Suhash Ranjan Dey, Alain Hazotte, Emmanuel Bouzy

Multiscale γ variant selection in a quaternary near-γ Ti-Al alloy

Journal:	*Philosophical Magazine & Philosophical Magazine Letters*
Manuscript ID:	TPHM-05-Oct-0470.R1
Journal Selection:	Philosophical Magazine
Date Submitted by the Author:	02-Mar-2006
Complete List of Authors:	DEY, Suhash; University of Metz, LETAM HAZOTTE, Alain; University of Metz, LETAM BOUZY, Emmanuel; University of Metz, LETAM
Keywords:	titanium aluminides, interfaces, microstructure, TEM
Keywords (user supplied):	misorientation

Multiscale γ variant selection in a quaternary near-γ Ti-Al alloy

S.R. Dey, A. Hazotte* and E. Bouzy

Laboratoire d'Etude des Textures et Application aux Matériaux, UMR-CNRS 7078, Université Paul-Verlaine, Metz, 57012 France

Abstract

Classical EBSD/SEM technique and a novel approach based on computer-aided collection and indexing of TEM Kikuchi patterns were used to study the γ variant and γ|γ misorientation distributions in lamellar grains of a near γ TiAl alloy. Coarse and fine lamellar structures obtained by continuous cooling at two different rates were investigated. The two methods were complementary and reveal the presence of one-twin-dominant zones (OTDZ) in all grains of both samples. In agreement with previous works, these OTDZ were proposed to result from a mechanism of self-accommodation through twin-variant selection at the nucleation stage. Moreover, it has been pointed out that one γ order variant often appears to be dominant in a given OTDZ. As the previous mechanism can hardly explain this experimental evidence, the presence of back-stresses due to the grain confinement is proposed as a possible explanation. The statistical analysis of γ|γ misorientation distributions, de-correlated from the effect of the non-random distribution of γ variants, reveals that γ|γ interfaces in true-twin relationship are clearly predominant in the coarse lamellar structure, but not in the fine one. This difference is discussed on the basis of different growth mechanisms recently underlined and whose respective influences depend on the transformation driving force, i.e. on the cooling rate.

Keywords: Titanium aluminides; Interfaces; Microstructure; Misorientation; TEM

1. Introduction

TiAl alloys are prospective light weight materials for high-temperature applications. The most attractive ones, denoted 'near-γ alloys', contain large amounts of an ordered tetragonal phase, called γ (TiAl-based, $L1_0$ structure) and less than 10% of an ordered hexagonal phase, called α_2 (Ti_3Al-based, $D0_{19}$ structure). Solidification process or high temperature heat treatments of these alloys lead to a specific microstructure (see Figure 1 and Figure 3) in which the grains inherited from the high temperature disordered hcp α phase (A3 structure) show parallel plates of γ phase occasionally separated by thin α_2 layers. This extensively documented 'lamellar' microstructure (see for instance [1,2,3] and the following references) has received a considerable interest, since lamellae characteristics (colony size, phase amounts and lamellae thickness distribution) strongly influence the mechanical properties [4,5]. Their characterisation is also essential for clarifying the mechanism of the $\alpha \rightarrow \alpha_2 + \gamma$ phase transformation ; an acceptable model

Comment [d1]:

*Corresponding author. Tel.: +33-387-31-5644; Fax: +33-387-31-5377.
E-Mail address: alain.hazotte@univ-metz.fr (A. Hazotte).

of transformation is expected to give explanations for experimentally observed quantitative characteristics of the lamellae assembly.

Lamellae show precise lattice orientation relationships and interface inclinations. All α_2 lamellae of a given grain have the same orientation as their α parent crystal. The (0001) plane of the α_2 phase is parallel to one {111} plane of γ. Due to the tetragonality of the γ phase, six non-equivalent misorientations emerge as the direction $[\bar{1}10]_\gamma$ gets parallel to six equivalent directions of the $<11\bar{2}0>_{\alpha_2}$ type. In other words, the γ lamellae appear in six specific orientation variants with respect to the orientation of α_2, or ex-α grain. Because of the symmetry of the parent hexagonal α phase, the misorientations between its inherited γ variants are exactly $k\times60°$ (k=0,1,…,5) rotations around the tetragonal $\langle 111\rangle_\gamma$ direction. Taking this information into account, there are four types of γ neighbours corresponding to the misorientation angles of:

- 0°, k=0 (i.e., two lamellae with the same orientation),
- 60°, k=1 or 5 (referred as 'pseudo-twins'),
- 120°, k=2 or 4 (with corresponding interface sometimes referred as '120°-rotational'),
- 180°, k=3 (true twins).

For conciseness, we will use the notations 0°, 60°, 120° and 180° to distinguish between these different interfaces, respectively. In [2] 0° and 120° boundaries are called 'perfect fitting' and 'order domain related' interfaces, respectively. The six orientation variants fall into two groups of three, the variants of one group being mutually related by 120° rotations. Their orientations would be symmetrically equivalent if the symmetry of γ were cubic; in that case, only two γ variants in twin relationship could be distinguished in a given grain. In the following, the six orientations variants issued from a single α grain will therefore be noted γ_1, γ_2, γ_3, γ_{1T}, γ_{2T} and γ_{3T}.

Because of the tetragonality of the unit cell (c/a ≅ 1.02), the angles between the $<110>_\gamma$ and $<101>_\gamma$ directions are not exactly 60° [6], consequently, the different {111} γ/γ interfaces do not match perfectly. This mismatch induces shear strains which could be partially relaxed by interfacial dislocations [7].

With this specific set of orientation relationships and boundary plane inclinations, the $\gamma|\gamma$ boundary distribution is essentially reduced to the frequency of occurrence of the four possible interfaces. It is known from earlier studies [2,6, 8-12] that this occurrence is not random and that the twin boundaries are often over-represented. However, because of experimental difficulties, the number of interfaces investigated remained relatively small. For the same reasons, most studies focused on coarse lamellar microstructures resulting from slow heat treatments. However, mechanisms proposed for the $\alpha \rightarrow \alpha_2 + \gamma$ phase transformation led to expect that the statistics of variant distribution should depend on the transformation rate.

In this paper, we study the orientation relationships between α_2 and γ variants in a quaternary TiAl-based alloy with coarse and fine lamellar structures resulting from casting and from rapid continuous cooling, respectively. Their analysis is performed at two different scales, using both a classical electron back-scattered diffraction (EBSD) technique in a scanning electron microscope (SEM) and an original semi-

automatic method, which allows to collect large lattice orientation data sets from linear scans in a transmission electron microscope (TEM).

2. Experimental procedure

2.1. Material and samples

The material under study was a quaternary near-γ alloy with chemical composition Ti-48Al-2Cr-2Nb (at.%). Samples were cut out from a cylindrical bar of 16 mm in diameter and 80 mm in length produced by investment casting. The solidification process resulted in coarse fully lamellar $\gamma+\alpha_2$ grains, with their lamellae mostly parallel to the bar axis. Thus, sections perpendicular to this axis contain numerous lamellar colonies with their interfaces roughly perpendicular to the surface; as commented thereafter, this will considerably enhance our statistical analysis. Two samples were analysed: one in the as-cast structure showed in Figure 1(a), and one submitted to an additional heat treatment of 30 min. at 1380°C (i.e. above the α transus) under argon, followed by a quench in sand (sand-quenched sample; Figure 1(b)). This second sample was extracted from a larger set of specimen submitted to different cooling rates leading to various microstructures [13]. It has been chosen for the present study since it corresponds to the highest cooling rate which enables to conserve significant amounts of fine lamellar structures coexisting with Widmanstätten laths and some feathery-like zones.

Surfaces for scanning electron microscopy (SEM) imaging and EBSD investigations were prepared by electropolishing with the electrolytic solution (60 vol.% methanol, 35 vol.% 2-ethoxy ethanol, and 5 vol.% perchloric acid (purity 70%)), using 100 mA of current and 17 V of voltage at –15°C. SEM images and EBSD mapping were performed on a JEOL JSM-6500F microscope equipped with a field emission-gun (FEG-SEM) and the Channel 5™ system developed by HKL®.

Thin foils for transmission electron microscopy (TEM) were prepared by mechanical polishing and subsequent electrolytic etching in the electrolytic solution reported above, using 50V of voltage. Samples were investigated using a Philips CM 200 operating at the nominal voltage of 200kV. A LaB_6 cathode was used as the electron source. Kikuchi diffraction patterns were obtained in the nano-probe mode, with a beam convergence angle of about 3°. They were recorded using a 1K x 1K Gatan 791 slow scan CCD camera mounted above the viewing chamber. The transmission microscope used was equipped with an original system named EP developed at LETAM and discussed below.

2.2. TEM observation and variant detection

The methods for determination of the six possible γ variants by TEM used in the previous studies were based either on spot diffraction patterns or on CBED patterns. The former needs to tilt the specimen to at least two zone axes, in order to avoid any ambiguous determination of the γ variants [14]. Its main advantage is to allow to visualise the different variants by dark field imaging [2]. Its major limitation is the low accuracy of the measured misorientations (few degrees). The latter method needs to tilt the specimen to a peculiar zone axis in order to index the Holz lines of the CBED pattern [10]. One CBED pattern is sufficient

to determine unambiguously the γ variant. But this method is manual and consequently tedious and time consuming.

The method used in the present study is based on the analysis of Kikuchi patterns sampled along a electron beam line scan. Collection, recording and subsequent correction of the patterns were done automatically, using an original software package described elsewhere [15,16].

This method allows automatic and rapid identification and orientation determination of α_2 phase and twin groups of γ. However, discrimination of order variants in each γ group is more delicate, since the patterns from one group of variants are nearly geometrically identical. Indeed the γ phase is tetragonal but with a c/a ratio very close to 1 (c/a≈1.02) and thus, the tetragonal distortion of the Kikuchi patterns is too small to distinguish the variants belonging to the same twin group. To differentiate between them, we used superlattice reflections in Kikuchi patterns, which appear when h+k=2n and h, k, l are not all odd or not all even. (see Figure 2 for an illustration). In principle, our software allows for fully automatic orientation determination of these superlattice bands. However, in the present case it was not sensitive enough to detect differences as small as those between the patterns of one γ group. Therefore, although the collection, enhancement of Kikuchi patterns and identification of α_2, γ and γ^T phases were performed automatically along a line roughly perpendicular to the lamellae, the order variant identification was made *a posteriori* by visual inspection. With an effective camera length of 82.2 mm, one Kikuchi pattern was sufficient for unambiguous identification of a γ orientation variant. Attribution of its orientation to each lamella observed in bright field mode is done *a posteriori*, using the contamination trace along the analysed profile (see Figure 3).

This semi-automatic method has the advantage of speed. Consequently large data collection have been performed for the different heat treated alloys. A second major advantage of the technique is that it allows very precise orientation determination, with an angular accuracy of nearly 0.2° [15]. Moreover, the main advantage of this technique for the present study is its very good spatial resolution. In principle, it is in the order of the spot size. To reproduce the characteristics of the microstructure at a very fine scale, a probe size of 5 nm and an electron beam scan step of 10 nm were chosen. Subsequent inspection of the bright field image showed that the lamellae are well detected, except for some of the narrowest α_2 lamellae. Indeed, the Kikuchi patterns of α_2 phase often appear rather diffuse. In addition, the interfaces could be not exactly parallel to the beam, reducing the resolution due to the superimposition of diffraction patterns originating from two neighbouring lamellae.

2.3 *EBSD analysis*

Electron back-scattered diffraction in a scanning electron microscope (SEM/EBSD) is a now well-established technique, which allows to automatically identify crystalline phases and to determine their crystallographic orientations over large areas on plane surfaces of bulk materials. It is based on the fast

automatic indexing of Kikuchi patterns successively acquired by scanning the surface under specific diffraction conditions (see for instance [17] for a general presentation).

In case of TiAl-based alloys, it is impossible to geometrically distinguish the Kikuchi patterns of the variants belonging to the same twin group, in SEM as in TEM. Moreover, the superlattice bands discussed before, which allow to distinguish these order variants by TEM, have a too low intensity ratio in comparison with the inelastic background to be detected even visually in classical SEM/EBSD patterns. An attempt to identify them was made by Pouchou et al. [18], who showed that it can only be possible under very specific experimental conditions (distance specimen–detection screen doubled, large beam intensity and large acquisition time in manual mode). They would not have been compatible with the large areas mapping in which we were interested in the present study. Consequently, the γ phase was classically indexed in automatic mode as a cubic system, i.e. only the two twin variants discussed before can be detected in a given grain. Elsewhere, the accuracy of the misorientation measurement can not be expected better than 1°.

The spatial resolution of SEM/EBSD is a function of the atomic number of the material, beam accelerating voltage, specimen tilt and probe size. For a FEG-SEM, it is found to be typically about 50 nm for aluminium in the direction parallel to the tilt axis (it is about three times larger in the orthogonal direction of the specimen surface) [19]. Consequently, with regard to the typical scale of microstructures, we chose to use a very small probe size in order to avoid as far as possible the superimposition of Kikuchi patterns that results in non-indexing when there is not a significant difference in intensity of the patterns. Nevertheless, the SEM/EBSD method was expected to fail to identify the α_2 lamellae in most cases , except for the very large ones and, concerning the γ phase of both cubic variants, indexing ambiguity was also expected *a priori* to occur sometimes, especially for the finer structure. But the objective of the present SEM/EBSD study was not to reproduce the lamellae microstructure at very fine scale, which was devoted to the TEM study. On the contrary, it aims to investigate the microstructure at larger scale. For this reason, we chose to use a large step size of about 2 microns.

3. Results

3.1. Orientation heterogeneity at the grain scale

When looking carefully at the succession of γ variants identified in Figure 3, it can be detected that the distribution of these variants along the ≈14μm long linear scan shows the predominance of one twin group, i.e. γ_1, γ_2 and γ_3, over the other one, i.e. γ_{1T}, γ_{2T} and γ_{3T}. This fact has been confirmed for several scans recorded on both as-cast and sand-quenched samples. It is exemplified on Figure 4. In this figure, the representation has been chosen to discriminate visually the γ variants of the two twin-groups. It becomes evident that, within a given grain, one of the two twin-groups is dominant over a region of several microns, then the second can become the major one further along the same scan.

Figure 5(a) and Figure 6 report γ orientation maps obtained through SEM/EBSD on large areas of the as-cast and sand-quenched samples, respectively. In opposition to what was expected in §.2.3, most Kikuchi

patterns in the lamellar zones were sufficiently sharp to easily index γ phase when assuming a cubic symmetry. This leads to detect several regions in a given grain, each of them being attributed to one of the two possible twin-groups. As an illustration, Figure 5(b) shows that the misorientations between two regions effectively corresponds to the one relative to γ twins, i.e. 60°. With regard to their size, it is clear for us that these regions should be related to the one-twin-dominant zones (OTDZ) pointed out by TEM scan analysis. In such OTDZ, the dominance of one twin variant will result in a sharp mean Kikuchi pattern, even if the electron spot cover several γ lamellae, as it is often the case in the sand-quenched structure. Therefore, SEM/EBSD technique reveals to be complementary to TEM approach when concerned with the analysis of γ variant distribution in lamellar TiAl-based alloys. The distribution and origin of these OTDZ will be discussed further.

3.2. Variant statistics at the lamellae scale

Table 1 collects the mean phase characteristics measured for all linear scans along both the as-cast (a) and the sand-quenched (b) samples. The linear fraction of γ (or α_2) phase is defined as the ratio of the line length within γ (or α_2) phase divided by the total length analysed. It is a non-biased estimator of the volume fraction of γ (or α_2) phase. For the as-cast sample, the measured phase volume fractions (3.2% of α_2) are close to the equilibrium values calculated for this alloy [20], while the ones for sand-quenched sample (18.9% of α_2) indicate that the alloy is far from thermodynamic equilibrium at the end of the fast cooling process. As expected, the sand-quenched structure is finer than the as-cast one. Due to the difference in phase amounts, the fineness of the quenched structure is more evident for γ lamellae. One important difference between the two microstructures concerns the number of γ layers between two α_2 lamellae. In the as-cast sample, it ranges most of the time between one and four, although it can be found considerably larger in some cases. The average number is 3.76, leading to a mean inter-space between α_2 lamellae equal to 1.48 μm. In the sand-quenched sample, these values drop to 1.39 and 0.20 μm, respectively. It is possible to compare the mean values of α_2 inter-space with those measured in a previous study by quantitative analysis of back-scattered electron images of samples cooled at different rates [20]. This gives a rough estimation of the mean cooling rates in the transformation range (i.e. between 1380°C and 1000°C), which are of the order of 50°C/min for the as-cast sample and of 1000°C/min for the sand-quenched one.

In terms of variant distributions, the existence of large OTDZ in a given grain requires a very careful analysis of the orientation statistics extracted at the TEM scale. Evidently, their mean values can be largely biased, depending on the position of the observed region with respect to these OTDZs. More precisely, one can suspect large bias when concerned with the mean statistics of individual γ variants, while the statistics of local misorientation between neighbouring lamellae are expected to be more significant.

Table 2 collects statistics of number and width distribution of γ variants measured in both as-cast (a) and sand-quenched (b) samples. For the reasons discussed before, the reported data correspond only to

measurements within the two OTDZs indicated in Figure 4. The trends discussed below have been confirmed in other zones. As expected, data clearly show the predominance of one twin-group. This is exemplified by a higher number of lamellae of the dominant twin, but also by a larger mean size of the corresponding lamellae. This trend is confirmed for both samples, although it still appears more evident for the OTDZ of the sand-quenched sample. More surprisingly, statistics also suggests that one γ order variant seems to be more represented amongst the three variants of the local dominant twin-group (variant γ_3 for as-cast sample and γ_2 for sand-quenched one). Once again, this effect appears more evident in case of sand-quenched sample. It will be discussed hereafter.

Table 3 and Table 4 report statistics relative to the nature of γ|γ interfaces (a) and of the misorientation between two γ lamellae sandwiching an α_2 lamella in a γ|α_2|γ sequence (b), for both the as-cast and sand-quenched samples, respectively. This time, the experimental data concern the whole set of measurements along the different linear scans analysed in the present study. They are compared with theoretical random distributions by mean of classical Khi-2 factors, the definition of which is given in the appendix at the end of this article. In fact, two theoretical distributions have been used for the comparison, which have been called 'true-random' and 'weighted-random'. If γ variants would be uniformly distributed in a grain and if no correlation takes place between neighbouring lamellae ('true-random'), the distribution of 60°, 120° and 180° γ/γ interfaces would be 2/5, 2/5 and 1/5, respectively, while the distribution of 0°, 60°, 120° and 180° misorientations between γ lamellae in a γ|α_2|γ sequence would be 1/6, 2/6, 2/6 and 1/6, respectively. However, it has been shown here above that the experimental γ variant distribution is far to be uniform, and that large-scale effects affect their statistics. Thus, the expected misorientation distribution if there is no correlation between neighbours has to be weighted by taking into account the local frequencies of γ variants in the OTDZ. The formulae to calculate this theoretical 'weighted-random' distribution are also reported in the appendix. The frequencies of γ variants, $f(\gamma_j)$, used for the calculations have been taken from Table 2(a) and (b), which means that we assume that the statistics of the two OTDZs analysed in Table 2. Similar calculations have been done on other OTDZs showed similar trend of khi2 with slight variations make Table 2 to be representative of all the OTDZ in all grains. This is a strong assumption, but i) a complete analysis of the mean variant distribution over all OTDZs is impossible and ii) we expect that this partial analysis would help us to identify qualitative trends in the data. A comparison between the results of γ|γ interfaces distributions measured in the present study and those of previous works [2,10] is also showed in Figure 7. In that case, since the γ variant distributions found in others works are different and/or unknown, we used the theoretical ratio of 2:2:1 for comparison with random combination of equi-probable variants.

From Table 3(a) and Figure 7, it is clear that the true twin γ|γ boundaries are over-represented in the as-cast sample and that the pseudo-twin boundaries are rare. Khi-2 factors calculated for both the true and weighted random distributions shows a highly significant departure from randomness (as an indication, the Khi-2 values noted in parentheses correspond to the critical values above which the theoretical random models could be rejected with a risk of error of 10%). The prevalence of twin interfaces is in quantitative agreement with previous works (cf. Figure 7). However, the incidence of pseudo-twin 60° interfaces

observed in the present study appears lower that the results published in [2] and [10]. Obviously, the fact that the internal domain boundaries were also counted in our case can affect the observed percentage of 120° boundaries and, consequently, the frequencies of true- and pseudo-twins. In opposition, Table 3(b) indicates no clear correlation between γ lamellae sandwiching one α_2 lamella, as showed by the low values of Khi-2 factor, in particular when working with the weighted distribution.

Due to the low number of adjacent γ layers in the sand-quenched sample, the γ|γ interface statistics of Table 4(a) are poor. However, it seems that the measured γ|γ interface distribution tends to be more random, as also exemplified by Figure 7, as well as by the low and not clearly significant values of the Khi-2 factor. Figure 7 shows that this trend is particularly evident for the 180° interface, the proportion of which is significantly lowered. While the statistics of $\gamma|\alpha_2|\gamma$ sequences is higher, Table 4(b) also shows no correlation between γ lamellae sandwiching one α_2 lamella in the sand-quenched sample. In this case, the interest of using a weighted theoretical distribution is particularly exemplified. Indeed, the lower value -and consequently not significant- value of the weighted Khi-2 factor with respect to the random one points out that the apparent over-representation of the 0° misorientation is due to the presence of a largely predominant variant in the ODTZs rather than by a correlation between neighbouring lamellae.

4. Discussion

4.1. Orientation heterogeneity at the grain scale

The existence of large one-twin-dominant zones (OTDZ) within a given lamellar grain has been pointed out by other authors using TEM techniques [2,8-10][1]. As far as we know, this is the first time that these OTDZ are clearly related to the detection of twinned zones in EBSD maps. This relation has been explained before: the recorded Kikuchi pattern appears sharp and representative of the local dominant twin-group. Consequently, EBSD is a suitable technique to analyse the morphology and size distribution of these OTDZs. With regard to the very different initial α grain size of the two samples (cf. Figure 5(a) and Figure 6), a statistical analysis of the OTDZ size distribution has not been attempted in the present study. However, it can be qualitatively stated that OTDZ are mostly elongated along the lamellae direction and often spread across the original α grain. Their width appears very scattered. An original result of the present study is the evidence of OTDZs even in the case of fine lamellar microstructures developed through fast cooling rate. In a previous study [11,12], Zghal et al. found a random variant distribution in fine lamellar structures obtained by water quench of an already partially transformed sample. In their case, the fine γ lamellae were showed to develop from the pre-ordered α_2 phase. This is not the case in the present work. Indeed, for the estimated cooling rate involved by sand-quenching, the γ transformation has been showed to start over 1100°C [20], i.e. largely above the $\alpha \rightarrow \alpha_2$ ordering temperature. Moreover, the development of Widmanstätten laths in numerous grains of the fine lamellar structure has been fully studied in an other article [13] and is explained on the basis of a displacive transformation from the α phase.

[1] Note that the representation used in Figure 4 was firstly proposed in [8].

One possible explanation for the existence of OTDZs has been recently proposed by Zghal et al., stating that they are probably due to a mechanism of variant selection by stress relaxation [11]. More precisely, a just-transforming hcp α grain is submitted to stresses due to thermal contraction and to eigenstrains resulting from the previous transformation of neighbouring grain(s). The stress field is complex and depends on the grain morphology, crystallographic orientation and elastic anisotropy. It has been proposed that the first stage of α→γ transformation takes place through heterogeneous nucleation of fcc lamellae on grain boundaries [1]. In that case, it can be expected that one of the two available twin-variants will be favoured, if minimising the local elastic energy density. In other words, the presence of OTDZs would result from a mechanism of self-accommodation through variant selection, as already described in several alloy families encountering displacive solid phase transformations. From this point of view, the existence of several OTDZs in one grain could be either due to the initial stress field heterogeneity or/and to the compensation of stresses generated by the growth of the firstly-nucleated OTDZs (see next paragraph for this point). The fact that we observed OTDZs in both as-cast and sand-quenched samples seems to agree with this explanation. Indeed, the characteristics of OTDZs are expected to be more dependent on the microstructural features at the grain scale (topology, grain boundary roughness, anisotropy,…) than on the nucleation conditions. In addition, it is worthwhile to note that Zghal observed no OTDZ in a multi-layered single-crystal TiAl alloy ('PST' alloy) [2,8], which also pleads for the influence of grain confinement.

Recently, the preponderance of one γ order variant within a given OTDZ has been reported by Zghal et al. [11,12]. But it is for the first time that the present authors have evidenced this phenomenon for fast cooling rates also. The fact that it even seems to be stronger in that case will be discussed in the next paragraph. Zghal et al. [11] implicitly assume that this 'order selection' could result from the same stress relaxation mechanism effective for twin-group selection. This assumption appears more difficult to support. Indeed, if one except a few notable works proposing that the α–>γ transformation proceeds by simultaneous crystal structure change and ordering [21], the literature rather admits that γ lamellae nucleate from α phase in two successive steps [1] (cf. Figure 10(a) to (c) for a schematic illustration of the process): i) a nucleation (sometimes denoted 'pre-nucleation') step in which fine non-equilibrium fcc layers (γ*) spread over large distances, through an hcp->fcc displacive transformation without composition change ; the twin-group selection may occur at this stage; ii) an ordering (or 'γ nucleation') step, in which the γ* pre-nuclei order in three different γ ($L1_0$) variants; it requires chemical diffusion and is concomitant with lamellae growth; the order variant selection should occur at this stage. However, due to the particular topology of the microstructure (very fine lamellae crossing the grain), it is likely that the grain boundary stress state would play a negligible role in its further development. Hazzledine et al. [7,22] stated that, apart from the chemical driving force, the most important force to be taken into account during growth of this type of microstructure would be the elastic energy associated with lattice mismatch between α phase and the different γ order variants. Considering an α_2/γ lamellar microstructure as an infinite multilayer (i.e. free of grain boundary), Hazzledine calculated the stress and strain tensors for each lamella [22]. With this ideal configuration, the stress state is homogeneous within a given α_2 or γ_i lamella. It just depends on the volume fractions of

α_2 phase and γ order variants (γ_i and γ_i^T are equivalents from this point of view), but neither on the lamellae thickness nor on the relative position of each lamella with respect to the others. Using the formulae given in [22] and same input data, we calculated the evolution of elastic energy as a function of γ volume fraction. It is represented in Figure 8(a), for different proportions of γ order variants. The curve has the well known parabolic shape, indicating that mismatch stresses act as an hindering force during the first time of γ growth (up to 40 %), then as a driving force. The predominance of one variant is effectively showed to result in a decrease of the internal elastic energy, but this effect appears to be very low during the early stages of growth (about 2.4% of difference for 40 % of γ phase). Moreover, the energy decrease is the same whatever the variant selected. Consequently, although this decrease mismatch energy is one of the driving forces for the disappearance of order boundaries during long-term coarsening of near-γ microstructures [9], it is likely not at the origin of the order variant selection during growth observed in the present study. One alternative origin could be the presence of an additive stress component, not associated with the lattice mismatch, but resulting from the confinement of the γ^* lamellae within a grain. Indeed, the development of one OTDZ in a given α grain results in a global shear deformation of this grain (cf. Figure 9). In return, the grain confinement would generate internal stresses in the parent and neighbour α grains, but also in the OTDZ, in which they should be relatively homogeneous. As discussed before, this 'back-stress' can be partly relaxed by the activation of new OTDZ in both parent and neighbour grains. An other available relaxation mechanism is the selection of a favourable γ order variant within the growing lamellae set. As an illustration, Figure 8(b) reports the evolution of the elastic energy when superimposing a uniform shear stress to the mismatch ones. In that case, the total internal energy depends on the selected variant. However, the level of additional stress required to induced noticeable effects appears to be rather high (10GPa in the present example, i.e. about 3 times the magnitude of mismatch stresses calculated in [22]). Works are in progress to estimate the order of magnitude of the effective confinement stresses associated with an OTDZ.

4.2. *γ/γ misorientation statistics at the lamellae scale*

The statistical analysis of $\gamma|\gamma$ and $\gamma|(\alpha_2)|\gamma$ misorientations performed in the present study clearly shows the predominance of twin $\gamma|\gamma$ interfaces in the as-cast (slowly-cooled) sample. On the contrary, no strong correlation –apart from those resulting from the global variant distribution- were found, neither for $\gamma|\gamma$ interfaces in the sand-quenched-cast (rapidly-cooled) sample nor for $\gamma|(\alpha_2)|\gamma$ misorientations in both samples. The agreement between the present results and those of previous studies has been discussed above.

We think that these experimental evidences can be properly explained on the basis of the $\alpha\rightarrow$ lamellar($\gamma+\alpha_2$) transformation mechanisms successively described by several authors [1,2,9,11,12] and schematised in Figure 10. This Figure deliberately separates the different transformation steps, which are actually concomitant and interactive. Steps a to c (γ^* pre-nucleation, then γ ordering/growth) were discussed before. Step g is relative to $\alpha\rightarrow\alpha_2$ ordering which, due to the low chemical diffusivity of both γ and α_2 ordered phases, can be considered to stop the whole transformation process. Depending on the cooling

conditions, it can takes place at any time of the transformation sequence. In the case of the as-cast sample, it occurred close to the end of the growth stage, while growth was not fully completed in the case of the sand-quenched sample. For very rapid cooling conditions, ordering can even occur before the $\alpha \rightarrow \gamma$ transformation starts. The development of non-random $\gamma|\gamma$ interface statistics can take place *a priori* during either further growth (step d) or coarsening (steps e-f) stages of the transformation. In the literature, migration of $\gamma|\gamma$ order domain boundaries and of $\gamma|\alpha$ interfaces at almost constant phase volume fraction has already been proposed as a possible mechanism for the selection of low energy interfaces [9]. Although it could be effective for long-time high-temperature treatments (for instance HIPping), we think that it does not play a significant role for transformations taking place during relatively rapid continuous cooling. Indeed, in these conditions, the chemical driving force is likely dominant with regard to the interface energy of order domain boundaries or $\gamma|\alpha$ interfaces and even to the mismatch elastic energy (which, according to Hazzledine et al. is probably partly relaxed in the last time of growth [7,22]). Therefore, the interface statistics measured in the present work have to be analysed on the basis of nucleation and growth mechanisms only. But in that case, the difficulty is to explain the origin of the numerous $\gamma|\gamma$ interfaces observed in the material, in particular for slower cooling. Impingement of γ lamellae (i.e. disappearance of α lamellae) during growth, which is sometimes presented without discussion as a 'natural' process, is actually not evident to admit in the case of cooling treatments passing through the α–γ domain. Indeed, it would require that interfacial and elastic forces could easily counterbalance the chemical force which tends to stabilise the $\alpha|\gamma$ structure. At the light of these remarks, interface statistics may finally be explained through specific nucleation/growth mechanisms which were pointed out and described recently in the case of TiAl alloys [11,12]. Figure 10(d_a) to (d_c) describe three different and concurrent mechanisms which can be active during the growth of γ lamellae within a α grain (for legibility purpose, order domains have not been represented in these schemata). Mechanism d_a is the classical moving of existing $\gamma|\alpha$ interfaces assisted by diffusion and controlled by atom jumps across the interface [1] ; it is mostly active for slow cooling rates or low undercooling leading to coarse structures. Mechanism d_c, which is general in solid phase transformation, is the continuous nucleation and growth of new γ lamellae in the non-transformed α spaces. It will occur for a sufficiently high transformation driving force, i.e. rapid cooling rate or high undercooling. Mechanism d_b is more specific and involves the nucleation of lamellae along existing $\gamma|\alpha$ interfaces, in twin relationship with the neighbour lamella. Since these twins are thought to develop at lower temperatures, after an initial period of growth dominate by interface moving, their width appears lower than the one of the first lamella generation [11]. We think that the predominance of twin $\gamma|\gamma$ interfaces in the as-cast sample (Figure 5(a)), coupled with the lower disproportion between twins numbers than between twin mean width (Figure 4) is a signature of the activation of such mechanism. Inversely, the absence of misorientation correlation in the sand-quenched sample pleads for a mechanism mostly based on continuous nucleation and growth of independent lamellae.

Conclusion

The original combination of two techniques allowing to determine crystallographic orientations through automatic indexing of Kikuchi patterns from either transmission or scanning electron microscopy proved to be powerful to analyse the multi-scale heterogeneity of γ variant distribution in near-γ TiAl alloys with a lamellar structure.

The division of lamellar grains in successive large one-twin-dominant zones (OTDZs), which can be suspected from careful and tedious thin foil analysis, can be easily and clearly confirmed by EBSD/SEM mapping over wider areas. Although the presence of such OTDZs has already been reported for long-term heat treated samples, it is the first time that they are observed in case of samples resulting from rapid continuous cooling from the α domain. In agreement with other authors, we proposed that they can be due to the accommodation of internal (thermal and eigenstrain) stresses, through twin-variant selection at the nucleation stage. As theoretical analyses showed that the distribution of γ variants influences the mechanical behaviour of these alloys, it is likely that the apparently systematic presence of OTDZs will also affect this behaviour. The present work also pointed out the predominance of one γ order variant amongst the three possible in a given OTDZ. Although EBSD/SEM is of no help in that case (i.e. the experimental evidence remains statistically poor), this fact was evidenced in several zones of both rapidly and slowly cooled samples. For reasons discussed before, we do not think that it can be explained by the self-accommodation mechanism advanced for OTDZs development. The alternative mechanism that we propose (selection of favourable variant to relax 'back-stresses' due to grain confinement) remains hypothetical and requires to be confirmed by proper micro-mechanics modelling approaches.

As a consequence of the non-random distribution of γ variants at the OTDZ scale, statistic analyses of variant and interface distributions at larger scales have to be carried out with great care. In particular, we are convinced that it can explain discrepancies between previous systematic studies in which this effect was not suspected. In the present work, we propose an –imperfect but useful- way to take it into account when analysing the different types of γ|γ interfaces and of γ|(α_2)|γ misorientations. It leads to confirm a significant over-representation of 'true-twin' γ|γ interfaces in the slowly cooled sample, but not in the quenched one. As re-arrangement of order domain boundaries and/or γ|α interfaces can hardly explain this phenomenon in case of lamellar structures resulting from continuous cooling, we prefer to assume a mechanism of twin nucleation at growing interfaces recently proposed by Zghal et al. [10]. Once again, it could be interesting to re-investigate some previous experimental results at the light of this recent knowledge upon lamella growth mechanisms. The influence of the phenomena occurring at the coarsening stage of the $\alpha \rightarrow \text{lamellar}(\alpha_2 + \gamma)$ transformation has perhaps been overestimated in the past.

Acknowledgements

The authors are indebted to Dr S. Naka, who offered the heat treatment facilities of ONERA research center. They are grateful to Drs J.J. Fundenberger (LETAM) and A. Morawiec (Institute of Metallurgy and

Materials, Kraków) for their help in the development and use of EP software, as well as to Dr. M. Humbert (LETAM) for fruitful discussions. S.R. Dey thanks the Regional Council of Lorraine for partial financial support of his Ph.D. work.

Appendix : Different formulae used for the statistics analysis of Table 3 and Table 4

Definition of Khi-2 factor : the Khi-2 factor (χ^2) is a classical tool in the field of statistics science. It allows to test the agreement between an experimental distribution and a theoretical one. Starting from a class distribution (number of occurrences per class), it is calculated as

$$\chi^2 = \sum_{i=1}^{k} \frac{\left[N_{\exp}(i) - N_{the}(i)\right]^2}{N_{the}(i)},$$

where k is the total number of classes, and $N_{exp}(i)$ and $N_{the}(i)$ are the number of experimental and theoretical occurrences in class i, respectively. If the experimental sample is actually extracted from a population following the theoretical model, the probabilistic density function of χ^2 is known. It is a function of χ^2 and of a parameter called 'degrees of freedom' (d.f. in Tables 3 and 4), which expresses the quantity of independent information offered by the class distribution. In the present case, d.f. = k-1. Thus, the theoretical model tested can be rejected if the calculated value of χ^2 is greater than a critical value above which the occurrence of this value becomes improbable (the probability of getting a χ^2 value higher than the critical one, even though the sampled population actually follows the theoretical model, is called 'risk' (to wrongly reject the model); it has been chosen equal to 10 % in Tables 3 and 4).

Calculation of 'weighted-random' theoretical misorientation distributions :

In presence of a non-random distribution of the six possible γ variants in a given grain, but in the absence of any additional correlation between neighbouring lamellae, the 'weighted-random' frequencies of misorientations between two neighbouring γ lamellae (including 0° misorientation, i.e. two neighbours with the same orientation) can be calculated through the following relations :

$$p^*(0°) = \sum_{i=1}^{3}\left[f(\gamma_i)^2 + f(\gamma_{iT})^2\right];\ p^*(180°) = \sum_{i=1}^{3} 2.f(\gamma_i).f(\gamma_{iT})$$

$$p^*(120°) = \sum_{i=1}^{3}\sum_{k\neq i}\left[f(\gamma_i)\,f(\gamma_k) + f(\gamma_{iT})\,f(\gamma_{kT})\right];\ p^*(60°) = \sum_{i=1}^{3}\sum_{k\neq i}\left[f(\gamma_i)\,f(\gamma_{kT}) + f(\gamma_{iT})\,f(\gamma_k)\right]$$

where the $f(\gamma_j)$ are the variant frequencies (measured) and the $p^*(i°)$ are the estimated misorientations frequencies (see the main text for the definition of 0°, 60°, 120° and 180° misorientations). In the present work, this distribution has been used as the theoretical one for the study of $\gamma|(\alpha_2)|\gamma$ sequences. For uniform distribution of the γ variants (i.e. $f(\gamma_j)=1/6$, whatever j), $p^*(0°)$, $p^*(60°)$, $p^*(120°)$ and $p^*(180°)$ are equal to 1/6, 2/6, 2/6 and 1/6, respectively ('true-random' distribution). As two neighbouring lamellae of same γ variant (0° misorientation) lead to a vanishing γ|γ interface, the 'weighted-random' theoretical frequencies of γ|γ interfaces, $p'^*(\alpha°)$, were just obtained by calculating the relative frequencies of the other misorientations when excluding the 0° one (for instance, $p'^*(60°)$ is equal to $p^*(60°)/[\ p^*(60°)+\ p^*(120°)+\ p^*(180°)]$. The corresponding 'true-random' distribution is : $p^*(60°)= p^*(120°)=2/5$; $p^*(180°)=1/5$

REFERENCES

[1] Denquin A, Naka S. Acta Mater. 1996;44:343.

[2] Zghal S, Naka S, Couret A. Acta Mater. 1997;45:3005.

[3] Yamaguchi M, Inui H, Ito K. Acta Mater. 2000;48:307.

[4] Appel F, Wagner R. Mat. Sci. & Engg. R 1998;22:187.

[5] Dimiduk DM, Parthasarathy TA, Hazzledine PM. Intermetallics 2001;9:875.

[6] Inui H, Oh MH, Nakamura A, Yamaguchi M. Phil. Mag. A 1992;66:539.

[7] Shoykhet B, Grinfeld MA, Hazzledine PM. Acta Mater. 1998;46:3761.

[8] Zghal S. Ph.D. Dissertation. Université Paul Sabatier, Toulouse, 1st December 1997.

[9] Zghal S, Thomas M, Naka S, Couret A, Phil. Mag. Letters 2001;81:537.

[10] Chen SH, Schumacher G, Mukherji D, Frohberg G, Wahi RP. Scripta Mater. 2002;47:757.

[11] Zghal S, Thomas M, Naka S, Finel A, Couret A. Acta Mater. 2005;53:2653.

[12] Zghal S, Thomas M, Couret A. Intermetallics 2005;13:1008.

[13] Dey SR, Hazotte A, Bouzy E, Naka S. Acta Mater. 2005;53:3783.

[14] Jin Z, Gray III GT. Mater. Sci. & Engg. A. 1997;231:62.

[15] Morawiec A, Fundenberger JJ, Bouzy E, Lecomte JS. J. Appl. Cryst. 2002;35:287.

[16] Fundenberger JJ, Morawiec A, Bouzy E, Lecomte JS. Ultramicroscopy2003;96:127.

[17] Pouchou JL. In: Pouchou JL editor. 'L'analyse EBSD - Principes et applications', EDP Sciences, 2003.

[18] Pouchou JL, Ferrini A, Denquin A, Boivin D, Renollet Y, Gallais C. In: Pouchou JL editor. 'L'analyse EBSD - Principes et applications', EDP Sciences, 2003.p.51.

[19] Humphreys FJ. Scripta Mater. 2004;51:771.

[20] Charpentier M. Ph.D. Dissertation. INPL, Nancy, 15th September 2003.

[21] Zhang LC, Cheng TT, Aindow M. Acta mater. 2004; 52: 191

[22] Hazzledine PM. Intermetallics 1998;6:673.

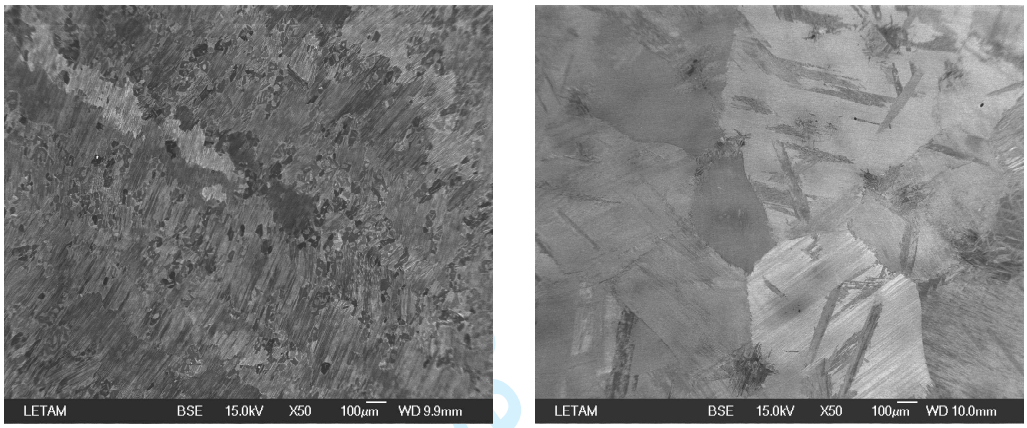

Figure 1. Back scattered electron micrographs of the as-cast (a) and sand-quenched (b) samples.

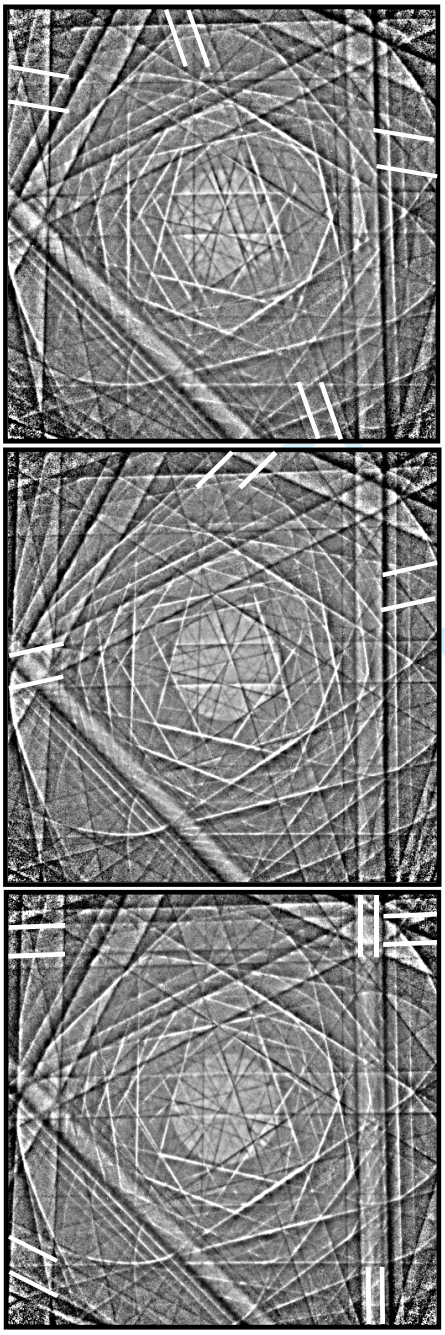

Figure 2. Kikuchi diffraction patterns of three γ variants from same twin group. White markers indicate some of the bands detectable only for a given variant. The linear dimensions of patterns used in practice are about twice bigger than here and the differences are more evident than in this reproduction

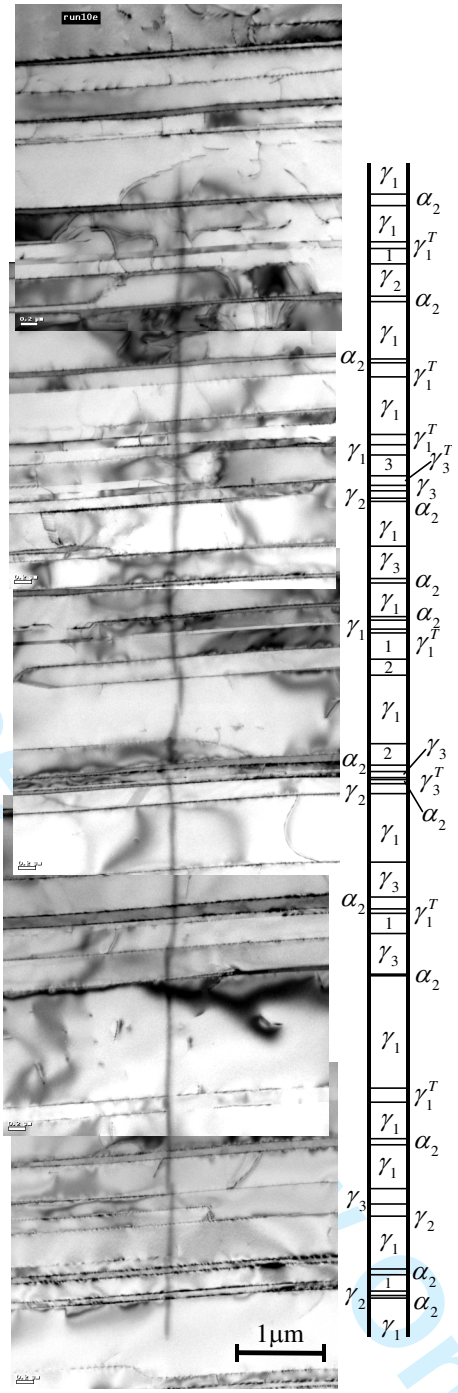

Figure 3. Lamellar microstructure of the as-cast sample, with the contamination mark of one of the linear scan and the detected phases/variants. The numbers '1', '2' and '3' mean the same as γ_1, γ_2 and γ_3, respectively.

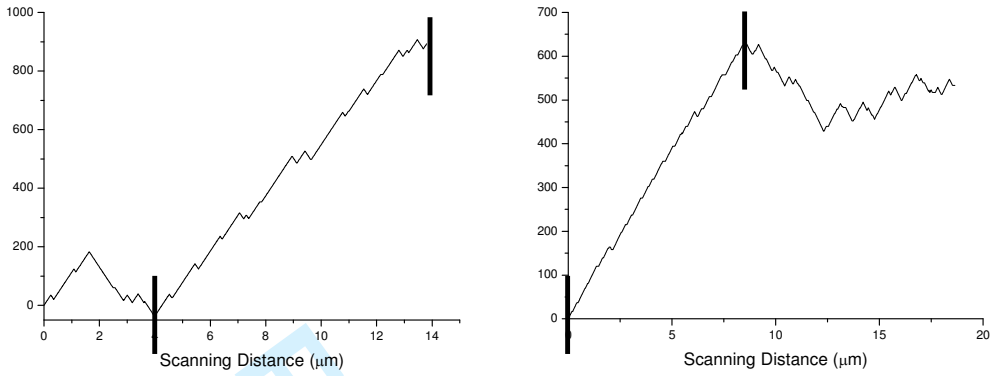

Figure 4. Distribution of γ twin variants over two TEM linear scans recorded on the as-cast **(a)** and sand-quench **(b)** samples. In this representation, each point corresponds to one indexed pixel (x-scale in μm); from left to right, the y value is incremented by 1 if the pixel belongs to one variant of a given γ twin group (for ex. γ_1, γ_2 or γ_3), decreased by 1 if it belongs to the other, and kept constant if it belongs to α_2 phase. Vertical bars indicate the OTDZ from which the statistics of Table 2 have been extracted.

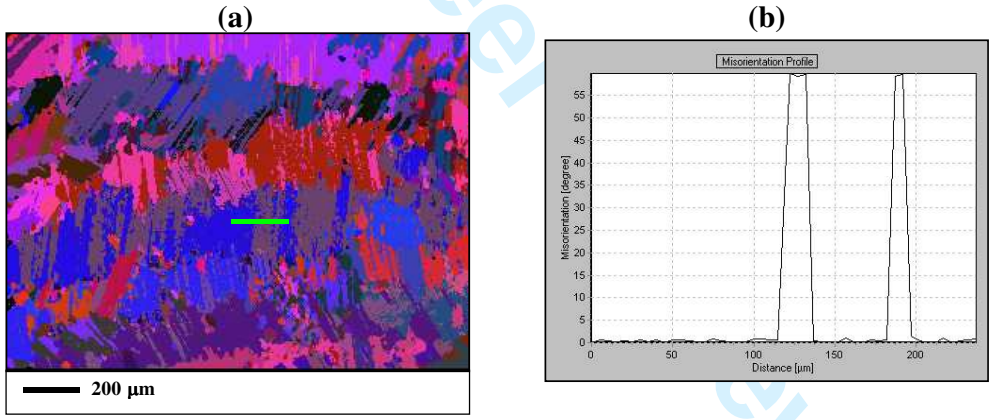

Figure 5. (a) γ orientation map obtained through SEM/EBSD on the as-cast alloy (each colour corresponds to a given crystallographic orientation with respect to a co-ordinate system of reference); note that only two colours are generally found in a given columnar grain; **(b)** evolution of misorientation angle along the line reported on (a) (the reference for misorientation calculation is the first pixel; minimum is 0° and maximum is 60°).

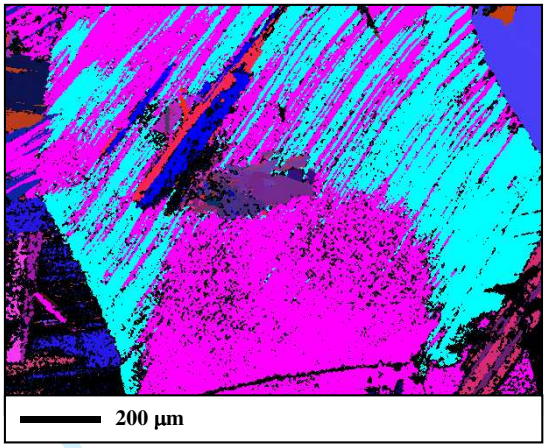

Figure 6. γ orientation map obtained through SEM/EBSD on the sand-quenched alloy.

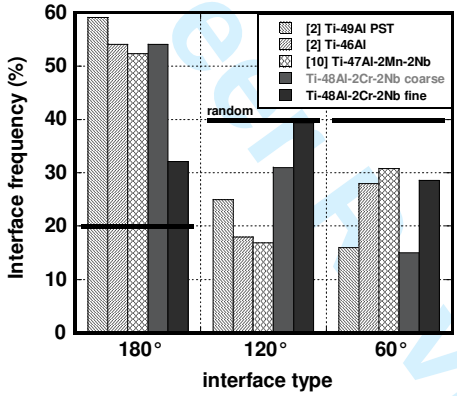

Figure 7. Comparison of the γ/γ interface frequencies measured in the present study with results from previous studies and with expected frequencies in case of randomness.

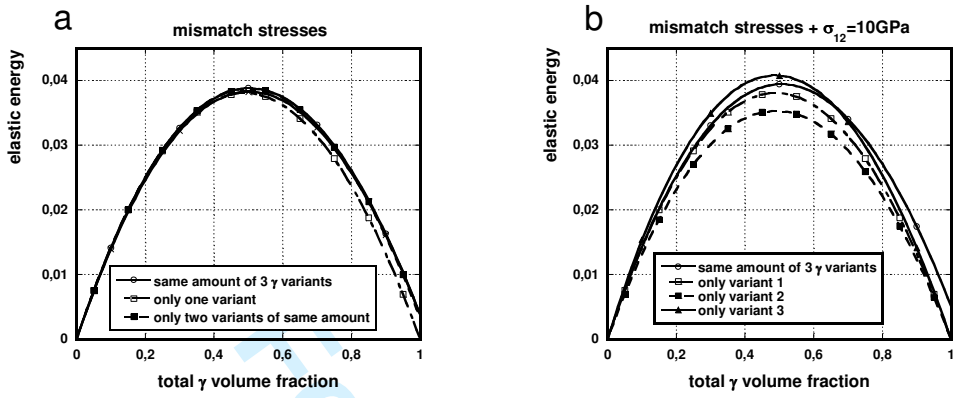

Figure 8. (a) Evolution of the mismatch elastic energy of a α_2/γ multi-layer as a function of the γ phase volume fraction (calculations based on [7]; **(b)** same evolution when superimposing an homogeneous shear stress of magnitude 10 Gpa.

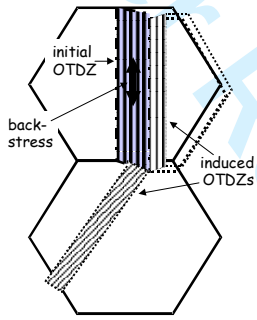

Figure 9. Schematisation of the origin of back-stress in an OTDZ.

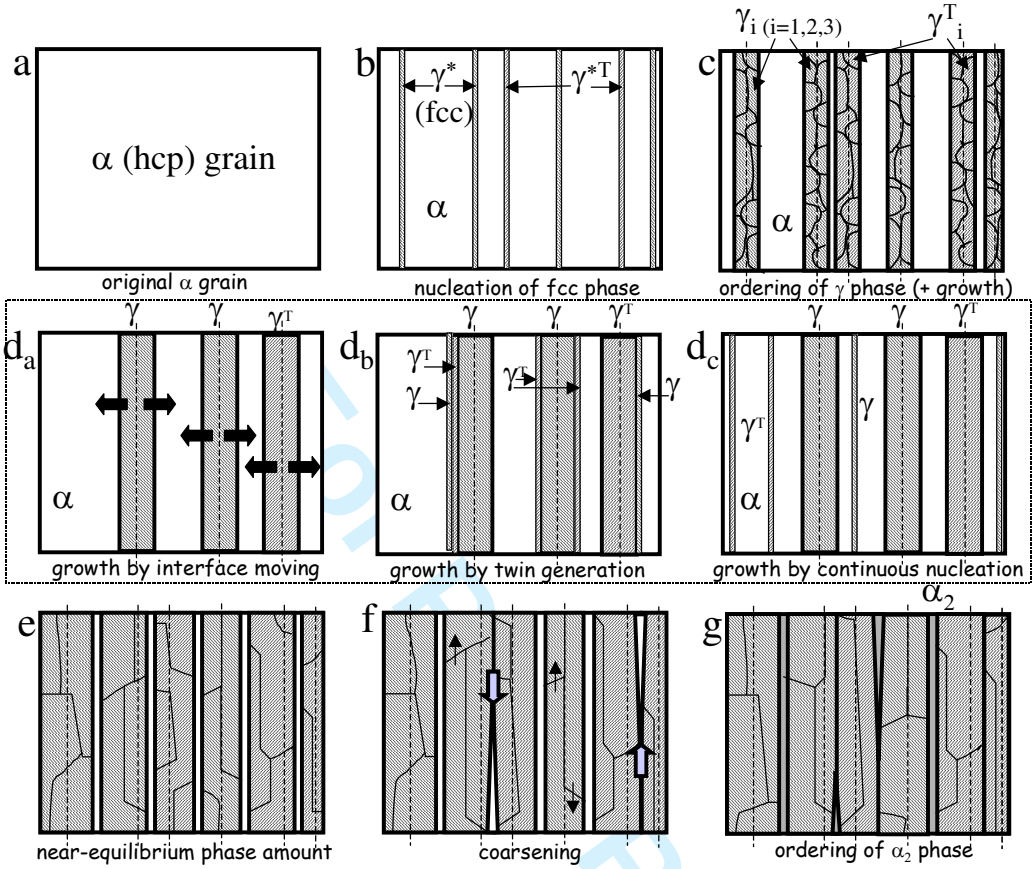

Figure 10. Schematic transformation sequence from the initial α grain to the final $\gamma + \alpha_2$ lamellar structure; for legibility purpose, order domains are not represented in Figure d_a to d_c; see the text for details.

Table 1. Statistics relative to the mean phase characteristics of the as cast (a) and sand-quenched (b) samples.

a		As-cast
α_2 phase	mean width (nm)	63.5 ± 2.24
	linear fraction (%)	3.2
γ phase	mean width (nm)	392.8 ± 9.20
	linear fraction (%)	96.8
mean number of γ lamellae between two α_2 lamellae		3.76

b		Sand-quenched
α_2 phase	mean width (nm)	52.9 ± 8.32
	linear fraction (%)	18.9
γ phase	mean width (nm)	145.5 ± 17.71
	linear fraction (%)	81.1
mean number of γ lamellae between two α_2 lamellae		1.39

Table 2. Number and width of γ variants measured in one OTDZ of the as-cast (a) and sand-quenched (b) samples.

a	As-cast (one OTDZ)					
total lamellae number	32					
γ variant	γ1	γ2	γ3	γ1T	γ2T	γ3T
number	5	5	11	3	4	4
%	15.6	15.6	34.4	9.4	12.5	12.5
% twin	65.6			34.4		
mean width (nm)	174	309	510	149	145	121
twin mean width (nm)	382			138		
linear fraction (%)	9.1	16.2	58.8	4.7	6.1	3.3
twin linear fraction (%)	84.2			15.8		

b	Sand-quenched (one OTDZ)					
total lamellae number	37					
γ variant	γ1	γ2	γ3	γ1T	γ2T	γ3T
number	5	28	1	1	1	1
%	13.5	75.7	2.7	2.7	2.7	2.7
% twin	91.9			8.1		
mean width (nm)	129	198	60	110	20	60
twin mean width (nm)	184			63		
linear fraction (%)	9.5	86.9	0.9	1.6	0.3	0.9
twin linear fraction (%)	97.2			2.8		

Table 3. Statistics relative to the nature of γ/γ interfaces (a) and of γ vs γ misorientations in γ/(α_2)/γ sequences (b) in the as-cast sample; see text and appendix for the details in Khi-2 factors.

a	As-cast		
number of γ/γ interfaces	298		
type of γ/γ interfaces	180° (TT)	120° (OD)	60° (PT)
exper. number	161	93	44
%	54.0	31.2	14.8
true random %	20.0	40.0	40.0
Khi2 factor (2 d.f.)	**225.7** *(5.99)*		
weighted random %	19.5	43.1	37.4
Khi2 factor (2 d.f.)	**233.7** *(5.99)*		

b	As-cast			
number of γ/(α_2)/γ sequences	95			
γ vs γ misorientation	180° (TT)	120° (OD)	60° (PT)	0° (PF)
exp.number	10	29	29	31
%	10.5	30.5	30.5	32.6
true random %	16.7	33.3	33.3	16.7
Khi2 factor (3 d.f.)	**17.3** *(7.82)*			
weighted random %	15.4	34.2	29.7	20.7
Khi2 factor (3 d.f.)	**8.4** *(7.82)*			

Table 4. Statistics relative to the nature of γ/γ interfaces (a) and of γ vs γ misorientations in γ/(α_2)/γ sequences (b) in the sand-quenched sample; see text and appendix for details.

a	Sand-quenched		
number of γ/γ interfaces	28		
type of γ/γ interfaces	180° (TT)	120° (OD)	60° (PT)
exper. number	9	11	8
%	32.1	39.3	28.6
true random %	20.0	40.0	40.0
Khi2 factor (2 d.f.)	**3** *(5.99)*		
weighted random %	12.2	63.3	24.5
Khi2 factor (2 d.f.)	**11.8** *(5.99)*		

b	Sand-quenched			
number of γ/(α_2)/γ sequences	56			
γ vs γ misorientation	180° (TT)	120° (OD)	60° (PT)	0° (PF)
exp.number	2	10	10	34
%	3.6	17.9	17.9	60.7
true random %	16.7	33.3	33.3	16.7
Khi2 factor (3 d.f.)	**79** *(7.82)*			
weighted random %	5.0	25.7	9.9	59.4
Khi2 factor (3 d.f.)	**5.12** *(7.82)*			